Geometries and interaction energies of toluene on Cs_xNA_{1-x} MOR

Nancy C. Cabana[1], Ramiro R. Serra[2], Alicia V. Boix[2], Pablo G. Bolcatto[*, 34]

[1] Facultad de Arquitectura, Diseño y Urbanismo (FADU,UNL)

[2] Instituto de Investigaciones en Catálisis y Petroquimica - INCAPE (FIQ,UNL-CONICET)

[3] Instituto de Matemática Aplicada del Litoral (UNL - CONICET)

[4] Facultad de Humanidades y Ciencias (FHUC,UNL)

Keywords: zeolite, mordenite, DFT, Differential Scanning Calorimetry, adsorption

[*]Corresponding author: pablo.bolcatto@santafe-conicet.gob.ar

Calculations for the geometries and energies of alkaline mordenites of the family Cs_xNA_{1-x} MOR $(x = 0, 0.25, 0.5, 0.75, 1)$ with and without toluene adsorbed and experiments of Differential Scanning Calorimetry (DSC) are reported. Firstly a structural stabilization of a pure silica zeolite was performed and then, four different structures for sodium substitutions were evaluated on a mordenite with a molar ratio Si/Al = 5. From the more stable matrix, a sequential incorporation of counterions from pure Na up to pure Cs was done. In each case the atoms were free to move inside the structure up to reach a local minimum of the total energy. Toluene was initially located in three different geometries and the energy optimization calculation relocate it properly. Mostly of the adsorption situations occurs when the electrons of the aromatic ring can interact with the counterions inside the main channel. The

This article has been accepted for publication and undergone full peer review but has not been through the copyediting, typesetting, pagination and proofreading process, which may lead to differences between this version and the Version of Record. Please cite this article as doi: 10.1002/pssb.202000131.

consideration of dispersive energy correction does not modify the basic physics of the adsorption process although it change the absolute values of the interaction energies. The DSC measurements were done for different amounts of toluene incorporated on two mordenites, one of them with only Na counterions and the other with a 7% of substitution by Cs. The technique gives the desorption energy and the results indicate that the incorporation of Cs enhances the adsorption ability of the zeolite. The overall theoretical results are in good agreement with experimental evidence and constitute a reliable basis to advance in the study of new functionalized materials.

1 Introduction

Strategies to reduce pollution have been matter of profuse multidisciplinary investigations along the recent decades. Particularly in combustion engines, there have been developed many catalysts able to reduce drastically the emission of nitrogen and carbon oxides [1-4]. However, the necessity to devel better materials and devices to reduce the emission of hydrocarbons (HCs) still remains due to incomplete combustion [5-7]. Many of these HCs (aromatic compounds, paraffins, olefins) are toxics and they are chemically photoactives in atmosphere. In consequence, investigations on the control of the emission using novel catalysts or adsorbent materials are of central importance nowadays. An idea in this sense is to use microporous materials -as for example zeolites-, which work as a tramp for HCs. The adsorption capacity, then depend to the localization of the adsorbed molecule and a balance between the acidity of the cations and the basicity of structural oxygen atoms. To achieve this, it is necessary to chemically modify the zeolites by incorporating cations and substituents and obtain promising systems for trapping HCs at low temperatures [8-10]. It was studied that the type of alkali cations provoke a change in the basic strength of the zeolite and increases in the order Li < Na < K < Rb < Cs and with this increases the hydrocarbon adsorption capacity. In these sense Su and Barthomeuf [11] showed that the amount of benzene

adsorbed in Faujasites X and Y exchanged with various alkaline cations increases parallel to oxygen basicity. Jabrouli et. al [12] also studied the effect of the different monovalent cations and transition metals such as silver and copper on the adsorption of toluene benzene and phenol on the FAU zeolite. On the other side, steric effects can influence dramatically the adsorption properties. In this sense, Keiji Itabashi *et al* [13] have found experimentally that water and benzene are less adsorbed in Rb-MOR than Na-MOR for the same Si/Al ratio. The explanation is because the ionic radius of Rb is greater than Na and then, the mean volume of the porous is reduced.

There is evidence of the interaction of the π^- electrons of the aromatic ring of some HCs with the zeolites from different techniques: Infrared spectroscopy (IR) [14], Utraviolet-Visible spectroscopy (UV-Vis) [15, 16], Nuclear Magnetic Resonance [17, 18], etc. However, the precise location of the adsorbent into the material is not a information easy to extract from experiments and therefore, *ab initio*$^-$ like calculations becomes an excellent tool to complement the comprehension of the physics involved. In particular, in a previous work a minimal cluster calculation was done in order to evaluate the adsorption of toluene on ZSM5 and mordenite zeolites exchanged with Cs [19].

The aim of this work is to systematically study, through first principles calculations and complementary experiments, different alternatives for the adsorption of a simple molecule as toluene in a sodium mordenite and cesium mordenites in which isomeric reactions are not expected. Na-MOR zeolite corresponds to microporous aluminosilicates family. Demuth et. al described its properties and characteristic [20]. There are many works that calculate the structure of zeolites exchanged with alkaline cations using DFT with different approaches for the exchange- correlation energy [20-24]. This kind of zeolites have main channels composed by rings of 12 members and secondary channels of 8, 5 and 4 members. In particular, the interaction between π^- electrons and the cations and the importance of the basic oxygen atoms in interaction with the methyl group within the principal channel is mainly analyzed from the theoretical point of view and from Differential Scanning Calorimetry experiments we obtain energies of desorption (or equivalently, adsorption). This study pursues the intention of giving quick clues about adsorption situations. It is strongly supported in a

complete structural stabilization of a familiy of adsorbent (the Cs_xNA_{1-x}MOR) not explored or achieved before. Thanks to this unavoidable step, the comprehension of experimental data of infrared spectroscopy, DSC (Differential Scanning Calorimetry), TPD (Temperature Program Desorption), flow-adsoprtion, porosity experiments for this family of zeolites [9, 19, 25] is now possible and it become a solid basis to advance in new and more refined theoretical calculations.

2 Methods

2.1 Theory

The fireball [26-29] code was used for the calculations. It is a tight-binding Density Functional Theory (DFT) implementation for periodic systems. Only valence electrons are considered and the effects of nucleus and core electrons are incorporated by pseudopotentials [30], fireball uses a numerical basis set for the valence states. The wavefunctions are localized around each atom in the system. They are different to zero only for distances lower than proper cutoff radii $r_i\ (i = s, p, d)$, which depend on the potentials selected. The standard Local Density Approximation (LDA) and the Generalized Gradient Approximation (GGA) for the exchange-correlation potential were used [31, 32].

In systems with large primitive or unit cell (as the zeolite are) it is common to restrict the sampling of the Brillouin-zone to the Γ point [20, 24]. However, here the calculation was done over 128 k^- points on the Brillouin-zone. The geometry of the structures was optimized at $T = 0$ K following a quenching method similar to the conjugate gradient method. The tolerance criteria for convergence was 10^{-4} eV/atom for the total energy of the primitive cell. The numerical error of the calculation is $\simeq 10$ meV [33, 34]. van der Waals corrections according to Grimme's DFT-D3 were used throughout all periodic calculations [35].

The efficiency and robustness of results arising from the approaches implemented in the

fireball code have been validated by hundreds of papers along the last decades [36]. However, a word of caution is worth pointing out here. The exchange-correlation approximations and the basis set used in this paper do not point to reach the most refined calculation of the structures. There are previous works concerning this topic, as for example the Refs. [20, 22, 24]. The focus here is to obtain a quick scenario of the phenomenology of the adsorption process which gives insights for the development of new materials potentially useful in catalytic processes. Therefore, firstly the calculation of the silica pure mordenite is presented in order to quantify the results of the method used in this work in comparison with well-stablished theoretical results. Then, structural optimizations of Cs_xNA_{1-x} MOR $(x = 0, 0.25, 0.5, 0.75, 1)$ were done and finally, the features of the adsorption of toluene are analyzed.

2.2 Experimental

Besides the theoretical analysis of geometries and energies of adsorption, experiments of Differential Scanning Calorimetry were done on the combined system (pure toluene + zeolite). The instrument used was a calorimeter Mettler Toledo 821. In the experiment 12 mg of zeolite was used, and different amounts of toluene was added in order change the micromoles of adsorbed toluene. The toluene amounts were: 0.5, 1.4, 3.2, 5.0, 8.0 and 10.0 mg, respectively. The zeolites impregnated with toluene were placed inside of an aluminum crucible, and it was heated under a N_2 gas flow (25 ml min^{-1}). The heating ramp used in the scanning was $10^{\circ}C\ min^{-1}$ from $25^{\circ}C$ to $450^{\circ}C$. In the same way zeolite or pure toluene were measured. Plots of desorption energy versus temperature (or time) were obtained and then the heats of transition, which are proportional to the area under the curve, were calculated.

From the heat of transition arising from DSC experiments, the desorption energy was calculated according to the following equation

$$E_{int} = E_{(zeolite+toluene)} - (E_{zeolite} + E_{toluene}), \quad (1)$$

being E_{int} the apparent desorption energy, $E_{(zeolite+toluene)}$ the energy of the adsorbed system, $E_{zeolite}$ the energy of the solid without treatment and $E_{toluene}$ the energy for the isolated toluene. Defined in this way, E_{int} is a desorption energy indeed so that a positive value means that the combined system is more stable than the sum of the isolated adsorbate and adsorbent.

3 Results

3.1 Structural stabilization of NaMOR

Before to analyze the adsorption properties it is necessary to find the optimal structure of the zeolite matrix for the calculation options selected in this study. The starting point is a pure silicate structure with an orthorhombic unit cell of $a = 18.256$ Å, $b = 20.534$ Å, $c = 7.542$ Å and $\alpha = \beta = \gamma = 90^{\circ}$ [37] (see Fig. 1). The corresponding monoclinic primitive cell is constituted by 96 atoms of O and 48 of Si. The monoclinic lattice parameters are $a' = b' = 13.90$ Å, $c' = 15.04$ Å and $\alpha' = \beta' = 90^{\circ}$ and $\gamma' = 97^{\circ}$. This primitive cell is indeed twice the minimal primitive cell since it was duplicated along c – axis, as it is shown in Fig. 1b. In this way it is assured that the toluene molecule will be free to find the best adsorption geometry inside the main channel.

In Table 1 is included the main interatomic distances and tetrehedral angles of the pure silica mordenite. Because the cutoff radius selected for the basis set, fireball-LDA results overestimate in about a 5% the relative distances (and consequently the optimal volume) as compared with codes based in plane waves. However, they maintain the correct shape since the angles are very close to the reference calculations [20]. On the other hand, fireball-GGA results are in a very good agreement with standard plane waves calculations. In this case the optimal volume is 4% greater than the IZA

database volume reported for silica pure mordenite [37].

In the next step we consider substitute some silicon atoms by aluminum up to reach a molar ratio Si/Al=5. It was done taking into consideration the Löwenstein's rule [38] i.e., avoiding that two consecutive tetrahedra AlO_4 are present in the structure, the four nonequivalent (T1, T2, T3 and T4) tetrahedra in the mordenite shows in Fig. 1c. There is not an unique way to obtain a mordenite with this molar ratio. Different models were explored being the substitution in T1 and T3 tetrahedra the more convenient combination in order to minimize the energy for both alternatives of the exchange-correlation energy approximation (Table 2). This result is in line with a previous one [39] in which were used different basis set and optimization strategy. The analysis is extended by exploring four different locations for the counterions, named NaMOR1, NaMOR2, NaMOR3 and NaMOR4, respectively. For the four models, aluminum atoms are in T1 and T3 tetrahedra and the sodium atoms are free to move from different initial locations. In order to find the optimal volume, different calculations were done changing the total volume but maintaining the shape and relative proportions. For the four models of Na-substitued mordenites the volume corresponding to the more stable energy is the same that the obtained for the pure silica case.

In the Table 3 the location of the counterions for the four models are presented. In all the cases four ions are finally placed at A-sites (following the notation of Mortier [40] indicated in Fig. 1c) or inside the secondary channel (SC, as in Ref. [41]). In NaMOR1 the other four counterions are two into the side pocket defined by the five-member ring (SP, C-sites) and two inside the main channel (MC, E-sites). NaMOR2 and NaMOR3 are very similar between them. They have four Na in E-like sites (MC). The difference is the location of the E-counterions along c -axis, while in NaMOR2 the cations are located in front of five- and six-members rings (site E^*), in NaMOR3 they are centered near the eight-member lateral ring. Lastly, in NaMOR4 the four remaining cations are located in C-sites (SP).

Demuth *et al* [20] calculated with LDA and GGA levels of approximation a mordenite with the same molar ratio that it is presented here (Si/Al = 5). While the places for the Al were T3 and T4 tetrahedrons, the final locations for the counterions were SC and MC. Here it is found the same final positions for the sodium atoms. On the other side, Chibani *et al* [24] also found that the SC and MC locations for the counterions together with aluminum atoms in T1 and T3 tetrahedrons are the energetically more favorable configuration. In this reference, the calculations were done with a molar ratio Si/Al = 47.

In Table 4 it is summarized the relevant distances for the different models of NaMOR, and it is also included experimental values of reference. Strictly, the comparison with natural o synthetic mordenites are not correct since the real mordenites do not have the same stechiometry that the theoretical structures: the composition of the natural mordenite reported by Alberti *et al* [42] is $(Na_{1.49}K_{2.80}Mg_{0.04}Ca_{2.05}Sr_{0.05})(Al_{8.98}Si_{39.13})O_{96}\cdot 29.07H_2O$, and the synthetic mordenite reported by Simoncin *et al* [43] is $Na_6Al_{6.02}Si_{42.02}O_{96}\cdot 19H_2O$. Nevertheless, the inclusion of experimental values is still a good reference to control the results arising from calculations.

3.2 Structural stabilization of Cs_xNA_{1-x} MOR

The next step is to stabilize new structures in which some Na counterions are replaced by Cs atoms. Maintaining the same molar Si/Al ratio, four new structures were optimized so that the sequence Cs_xNA_{1-x} MOR $(x = 0, 0.25, 0.50, 0.75, 1)$ is completed. The starting point for the structural stabilization was NaMOR3 $(x = 0)$, the more energetically stable structure.

The new Cs atoms were placed initially in E-sites and successively were occupying A-sites depending on the $x-$ fraction. In each case, the complete structure is free to move up to reach a new minimum. These calculations were performed for different volumes in order to find the new optimal primitive cell. Following the trends of the previous findings in the GGA (LDA) aproximation, the

optimal volume is in all the cases a 4% (15%) greater than the reference value for the silica pure matrix [37] as it can be observed in Fig. 2. Again, it is possible to be confident that, while this value is greater than the experimental data or more sophisticated calculations, is very robust and reliable itself to make comparisons if the same atomic basis set and options of calculations are unchanged.

In this process of structural stabilization the counterions travel through the matrix occupying new sites. Those that initially were in the main channel remain inside it (MC, E-sites). Nevertheless, because the Cs have greater ionic radius than the Na atoms, they change slightly their positions towards to the center of the channel. On the other hand, the atoms in A-sites moves to B-sites (both in SC) when the Na is replaced by a Cs. This fact is reflected in the right panel of Fig. 2b where the linear tendency of the optimal energy in function of x-fraction is broken for $x > 0.5$. However, the common feature is that in all the cases the counterions are located in MC and SC sites. Another remarkable feature is that for $x > 0.5$ the structure is not stable when the primitive cell is reduced. The reason is that due to the high ionic radius of the Cs atoms, the new counterions moves very near to oxygens of the matrix and trends to form oxides which distort in such way the structure that provoke the instability.

3.3 Toluene adsorption

In this section the geometries and energies of the toluene adsorbed in NaMOR1-4 and Cs_xNA_{1-x} MOR are presented. Due to the size of the toluene molecule, only adsorption inside the main channel is considered. However, it is possible to explore configurations which favor the interactions either the methyl group or the π -electrons with selected sites of the substrate. In particular, cations sites and oxygen atoms near Al-tetrahedra are supposed to be the more reactive sites. In consequence, three adsorption situations were considered. Calling π to the direction perpendicular to the plane of the aromatic ring and σ to the direction parallel to the ring and

coincident with the methyl group bonding, the three adsorption situations are: tolA: σ -direction parallel to $ab-$ plane and the methyl group pointed to the cations, tolB: σ -direction perpendicular to $ab-$ plane and $\pi-$ electrons not oriented to any cation, tolC: σ -direction perpendicular to $ab-$ plane and the $\pi-$ electron cloud rotated 90° respect to tolB situation.

In Fig. 3 the final geometries for the adsorption on NaMOR1-4 are presented. tolA-locations are the less realistic ones because the $\sigma-$ direction is perpendicular to the $c-$ axis, not being this the preferred orientation in real adsorption. Besides, in NaMOR2 and NaMOR3 the toluene is strongly locked by the counterions. In spite of that, toluene molecules always find a stable position. In NaMOR2, the adsorbate does not reach an equilibrium position when it is positioned as tolB and tolC. The reason is that the aromatic ring interacts such strongly with a particular ion in E-position that stress and deforms the structure excessively. In NaMOR3 this phenomena does not occur and the only structural difference compared with NaMOR2 is the position along $c-$ axis of the counterions inside the main channel, E^{*} instead E. As it is expected, in NaMOR4 the toluene remains almost in its initial position because it has no counterions to interact with.

The substitution of Na by Cs ions was done starting from the more stable structure, NaMOR3. In the figure 4 the final geometries of the toluene adsorbed in Cs_xNA_{1-x} MOR are shown. The case $x=0$ is again included for completeness. As previously, the denomination tolA, tolB and tolC refers to the initial orientation of the toluene molecule although in the selfconsistent process all the atoms (matrix plus adsorbate) are free to move up to reach the (local) minimum of the total energy. In tolA cases the toluene is tightly locked by the cation in MC which, while is stable for the calculations is expected to be a very improbable real situation. In tolB the $\pi-$ electrons seek a geometric orientation parallel to $b-$ direction. Due to steric hindrance of counterions with high ionic radius, as is the case of Cs, the molecule is shifted upwards and then the adsorption is weaker than the other cases. In turn, in tolC $\pi-$ electrons point to $a-$ direction which enhance the interaction with the counterions inside the main channel. For $x=0.75,1$, when the Cs cations migrate from A to B sites, occurs such

guest-host interaction that the whole structure is unstable.

The analysis of the geometries is complemented with the energies involved in each case. The adsorption energy is calculated as:

$$E_{ads} = E_{Cs_xNa_{1-x}MOR+tol} - E_{Cs_xNa_{1-x}MOR} + E_{tol} \quad (2)$$

where $E_{Cs_xNa_{1-x}MOR}$ and E_{tol} correspond to the energies of the Cs_xNA_{1-x} MOR and the toluene isolated, respectively, and $E_{Cs_xNa_{1-x}MOR+tol}$ is the energy of the complete interacting system. Thus, a negative value for E_{ads} means that the adsorbate is stable in the adsorption situation.

DFT methods does not include the van der Waals (vdW) dispersive energies in the selfconsistent process. This corrections are normally added through alternative (mostly empirical) models after achieved convergence in the DFT calculations[35, 46, 47]. Given that in the micropores of the MOR structures studied here the induced vdW-interactions maintain the toluene as a host it is possible to incorporate empirically the dispersion correction to the DFT results. In this work the vdW-dispersive corrections to the energy was incorporates following the reference [48]. In the latest version (referred to as DFT-D3), ab initio data has been successively refined for greater precision and less empiricism, so dispersion corrections are now available for all items, with improved overall performance. For the implementation, the fitted parameters are those arising from the dimeric results by using the widely probed PBE functional. The corrected dispersive adsorption energy is expressed as:

$$E_{ads}^{corr} = E_{ads} + E_{vdW} \quad (3)$$

The adsorption energies for all the NaMOR structures considered are summarized in table 5.

In NaMOR1, NaMOR3 and NaMOR4 it is possible to adsorb the toluene in any of the three orientations, being NaMOR1 the system that adsorbed the hydrocarbon more strongly. The adsorption of toluene on NaMOR4 is energetically less favorable due to the absence of extra network cations within the main channel. In the case of NaMOR2, which has four extra network cations in the main channel, toluene could only be adsorbed in one position (tolA) in opposition to what occurs in NaMOR3, which also has the same amount of counterions at MC. The differences between both structures resides mainly in the relative positions of the Na along the $c-axis$. In NaMOR2 are in sites more weakly bound to the network, then for the orientations tolB and tolC the force of the interaction between the Na and the toluene is such strong that destabilize the structure. In fact, the sodium cations act as a Lewis acid to form a strong interaction with the $\pi-$ electrons of toluene [9].

The calculations presented here give a negative dispersive energy correction of the order of 0.7-0.8 eV. This value is consistent with the correction of around 0.5 eV reported for similar (but not equal) mordenite systems [24, 46] and they do not change the relative conditions of adsorption.

Experiments of adsorption heat indicate a value of -0.23 eV for a mordenite with a molar ratio of 6.5 [19] and -1.39 eV for a structure with a molar ratio of 20 [49]. Experimentally is not possible to have access to the orientation of each adsorbed molecule inside a given zeolite and then the experimental value is an average of all the possible adsorption situations indeed. The whole range of values reported here is compatible with the experimental data. To inform a unique theoretical value requires an average. As the calculations were done at $T = 0$ K, a simple non-weighted average seems to be the option to give an early estimation of the strength of the adsorption. The LDA (GGA) average E_{ads} is -0.54 eV (-2.20 eV) and -1.25 eV (-3.01 eV) with the dispersive correction respectively. The simple average assumes that all the sites have the same probability to occur. This is clearly a drastic assumption even at $T = 0$ K. For example, while finally all the atoms are free to move until to reach a local minimum of energy, the initial position tolA is expected to favor a position chemically less probable and then its weight in the average will be overestimated. Besides, as the experiments are mostly done at room temperature, it is expected that the calculated strengths of the adsorption are

greater than the real ones. A more realistic estimation is to perform a Boltzmann-weighted average. This alternative means to combine DFT calculations with molecular dynamics (MD) [33, 34] or Monte Carlo [50] in order to incorporate temperature effects. In spite of this is not the scope of this particular analysis, a preliminary DFT-MD can be reported. For NaMOR3 matrix and setting the temperature of the system at $T = 298$ K, the variation in total energy ΔE is 1.2 eV/unit cell for tolA position, 0.6 eV/unit cell for tolB and 0.9 eV/unit cell for tolC. Therefore, as the Boltzman weight is $exp(-\Delta E / k_B T)$, the temperature-pondered average is very close to the tolB value since the other two apart enough to have a significant statistical weight. Similar behaviors to the other adsorbents are expected.

Lastly, the energy adsorption values for the Cs substitution are summarized in table 6. The zeolite which more strongly adsorbs toluene is that with $x = 0.25$ because there is a intermediate situation between a more favourable interaction with Cs counterions but still without a dramatic steric hindrance. The vdW correction in all the cases is about 0.8 eV, following the same trends that previous results.

It is known that the toluene molecule is preferentially adsorbed on the cations through the aromatic ring [12]. In turn, the cesium cation has a higher electron density than sodium, which could promote the greatest interaction with the toluene molecule. This was one of the factors that influenced the interaction with the aromatic molecule. In other works, such as the case of Jabrouli et al.[51] who studied the effect of the Si/Al ratio, since the interaction of toluene increases when the ratio decreases. In this sense, the mordenite studied has a Si/Al = 5 ratio which favors a greater number of cesium cations and therefore a greater interaction with toluene.

3.4 DSC experiment

In this section results of Differential Scanning Calorimetry (DSC) are presented for two different zeolites, NaMOR y CsNaMOR with a 7% of Cs in weight (which is equivalent to an

$x \simeq 0.3$). Three similar experiments were carried out for each combined system. Firstly, a drop of toluene is introduced in the crucible, then only the zeolite, and finally, the zeolite is successively impregnated with increasing amounts of toluene.

The interaction energy was calculated as indicated in the experimental section (Eq. 1). Due to the experiments measure the desorption, the value obtained has the opposite sign that the calculated with the Eq.(2). The results of E_{int} vs ξ, being ξ the ratio between the moles of toluene and zeolite moles are shown in Fig. (1). When the amount of toluene increases, the interaction (desorption) energy increase until a constant value is obtained. The crosspoint in which it happens gives count of the total amount of toluene adsorbed in the sample. It can be observed that the sample with cesium have higher energy of interaction than NaMOR sample (2.05 eV and 1.88 eV, respectively). This could be due to the fact that the cesium atom has an electronic density greater than of sodium, generating a higher interaction with the toluene molecule. These results have the same tendency as the theoretical results summarized in the tables 5 and 6. The Cs substitution implies a doble effect: increase both the interaction energy from 1.88 eV to 2.05 eV, and the total toluene adsorbed from $\xi = 12.0$ to $\xi = 12.4$.

4 Conclusions

Different substitutions for mordenite were analyzed using a tight-binding DFT approach. The structural optimization, i. e., the location of the cation atoms, was done at $T = 0$ K following a quenching method for the minimization of the total energy which is similar to the gradient conjugate method. For a molar ratio Si/Al = 5, which means the presence of 8 counterions in the primitive cell, the more stable structure for a sodium pure substitution is those in which 4 ions are located in the main channel. For this last case, two different options were evaluated (named, NaMOR2 and NaMOR3) being the more stable those in which the ions are located in front of the 8-members lateral ring (NaMOR3). Then the Cs_xNA_{1-x}MOR3 $(x = 0.25, 0.50 0.75, 1)$ structures were optimized before

the inclusion of toluene molecules. In the adsorption, the toluene prefers in most of the cases to orient π^- electrons in such way to optimize the interaction with ions inside the main channel. When this interaction is strong enough, the structure becomes unstable (tolB and tolC in NaMOR2 and tolC in Cs_xNA_{1-x}MOR3 $(x = 0.75,1)$. Differential Scanning Calorimetry experiments of toluene adsorbed on NaMOR and CsNaMOR indicates that the cesium enhances both the interaction energy as the total amount of toluene adsorbed if the substitution with Cs is around $x = 0.3$. The results are a combination of the option selected to the exchange-correlation potential and the basis set used. The geometries calculated with GGA are in excellent agreement with crystalline data but seem to overestimate the adsorption energies. On the other hand, LDA gives in general longer bonding distances and then molecule size and unit cells are greater than the experimental ones. However, LDA-adsorption energies are closer to the experimental data. Beyond the precise quantitative comparison between theory and experiments, the overall physical behavior for many geometries and adsorbate/adsorbent complexes is well addressed. Thus, the final insights constitute a reliable basis to advance in the study of other guest-host systems representing new functionalized materials.

Acknowledgements

The authors acknowledge the financial support of CONICET. This work was support under grants CAI+D 50120110100561LI (UNL) and PICT 2013-0354 (ANPCyT).

References

[1] P. M. More, M. k. Dongare, S. B. Umbarkar, P. Granger, and C. Dujardin, Catalysis Today **306**, 23–31 (2018).

[2] J. B. Lim, J. Shin, N. H. Ahn, I. Heo, and S. B. Hong, Applied Catalysis B: Environmental **267**, 118710 (2020).

[3] X. Zhang and Y. Yan, Royal Society open science **5**(8), 180587 (2018).

[4] T. H. Bae, M. R. Hudson, J. A. Mason, W. L. Queen, J. J. Dutton, K. Sumida, K. J. Micklash, S. S. Kaye, C. M. Brown, and J. R. Long, Energy & Environmental Science **6**(1), 128–138 (2013).

[5] P. Verma, S. Stevanovic, A. Zare, G. Dwivedi, T. Chu Van, M. Davidson, T. Rainey, R. J. Brown, and Z. D. Ristovski, Energies **12**(10), 1987 (2019).

[6] A. Tsolakis, M. Bogarra, and J. Herreros (2017).

[7] S. Elangovan, M. Ogura, Y. Zhang, N. Chino, and T. Okubo, Appl. Catal., B **57**(1), 31–36 (2005).

[8] F. Migliardini, F. Iucolano, D. Caputo, and P. Corbo, J. Chem. , 269694 (2015).

[9] R. M. Serra, E. E. Miró, M. K. Sapag, and A. V. Boix, Microporous Mesoporous Mater. **138**(1–3), 102–109 (2011).

[10] R. K. Maurya, R. K. Maurya, and Luby, Characteristics and control of low temperature combustion engines (Springer, 2018).

[11] B. L. Su and D. Barthomeuf, Zeolites **15**(5), 470–474 (1995).

[12] H. Jabraoui, I. Khalil, S. Lebègue, and M. Badawi, Molecular Systems Design & Engineering **4**(4), 882–892 (2019).

[13] K. Itabashi, A. Matsumoto, T. Ikeda, M. Kato, and K. Tsutsumi, Microporous Mesoporous Mater. **101**(1), 57–65 (2007).

[14] I. Graça, J. D. Comparot, S. Laforge, P. Magnoux, J. M. Lopes, M. F. Ribeiro, and F. Ramôa Ribeiro, Energ. Fuel. **23**(9), 4224–4230 (2009).

[15] S. Fukahori, H. Ichiura, T. Kitaoka, and H. Tanaka, Environ. Sci. Technol. **37**(5), 1048–1051 (2003).

[16] Y. T. Chua, P. C. Stair, J. B. Nicholas, W. Song, and J. F. Haw, J. Am. Chem. Soc. **125**(4), 866–867 (2003).

[17] C. Laborde-Boutet, G. Joly, A. Nicolaos, M. Thomas, and P. Magnoux, Ind. Eng. Chem. Res. **45**(20), 6758–6764 (2006).

[18] C. Laborde-Boutet, G. Joly, A. Nicolaos, M. Thomas, and P. Magnoux, Ind. Eng. Chem. Res. **45**(24), 8111–8116 (2006).

[19] R. M. Serra, E. E. Miró, P. G. Bolcatto, and A. V. Boix, Microporous Mesoporous Mater. **147**, 17 (2012).

[20] T. Demuth, J. Hafner, L. Benco, and H. Toulhoat, J. Phys. Chem., B **104**(19), 4593–4607 (2000).

[21] V. D. Dominguez-Soria, P. Calaminici, and A. Goursot, J. Chem. Phys. **127**, 154710 (2007).

[22] T. Bucko and J. Hafner, J. Catal. **329**, 32–48 (2015).

[23] F. d. S. Vilhena, R. M. Serra, A. V. Boix, G. B. Ferreira, and J. W. d. M. Carneiro, Comput. Theor. Chem. **1091**, 115–121 (2016).

[24] S. Chibani, M. Chebbi, S. LebÃ¨gue, T. BuÄ • ko, and M. Badawi, J. Chem. Phys. **144**(244705), 1–10 (2016).

[25] R. M. Serra, E. E. Miró, and A. V. Boix, Microporous Mesoporous Mater. **127**, 182–189 (2010).

[26] O. F. Sankey and D. J. Niklewski, Phys. Rev. B **40**, 3979–3995 (1989).

[27] A. A. Demkov, J. Ortega, O. F. Sankey, and M. P. Grumbach, Phys. Rev. B **52**, 1618–1630 (1995).

[28] J. P. Lewis, K. R. Glaesemann, G. A. Voth, J. Fritsch, A. A. Demkov, J. Ortega, and O. F. Sankey, Phys. Rev. B **64**, 195103 (2001).

[29] P. Jelínek, H. Wang, J. P. Lewis, O. F. Sankey, and J. Ortega, Phys. Rev. B **71**, 235101 (2005).

[30] D. R. Hamann, Phys. Rev. B **40**, 2980 (1989).

[31] A. D. Becke, Phys. Rev. A **38**(6), 3098 (1988).

[32] C. Lee, W. Yang, and R. G. Parr, Phys. Rev. B **37**(2), 785 (1988).

[33] S. C. Gómez-Carrillo and P. G. Bolcatto, Phys. Chem. Chem. Phys. **13**, 461 (2011).

[34] S. C. Gómez-Carrillo and P. G. Bolcatto, J. Phys.: Condens. Matter **25**, 045005 (2012).

[35] S. Grimme, J. Compt. Chem. **27**(15), 1787– –1799 (2006).

[36] J. P. Lewis, P. Jelíek, J. Ortega, A. A. Demkov, D. G. Trabada, B. Haycock, H. Wang, G. Adams, J. K. Tomfohr, E. Abad, H. Wang, and D. A. Drabold, Phys. Stat. Sol. (b) **248**, 1989–2007 (2011).

[37] C. Baerlocher and L. McCusker, Database of Zeolite Structures - IZA Structure Commission, accessed on January 6 2014.

[38] W. Löwenstein, Am. Miner. **39**(1-2), 92–96 (1954).

[39] N. C. Cabana, A. V. Boix, and P. G. Bolcatto, Anales AFA **25**(3), 1 (2014).

[40] W. Mortier, Compilation of Extra Framework Sites in Zeolites (Butterworths Sci. Ltd.: Guilord, 1982).

[41] L. Benco, T. Bucko, and J. Hafner, J. Catal. **277**, 104–116 (2011).

[42] A. Alberti, P. Davoli, and G. Z. Vezzalini, Kristallogr. **175**, 249 (1986).

[43] P. Simoncic and T. Armbruster, Am. Mineral **89**, 421–431 (2004).

[44] F. Birch, Phys. Rev. **71**(Jun), 809–824 (1947).

[45] F. D. Murnaghan, American Journal of Mathematics **59**(2), 235–260 (1937).

[46] A. M. Vos, X. Rozanska, R. A. Schoonheydt, R. A. van Santen, F. Hutschka, and J. Hafner, J. Am. Chem. Soc. **123**, 2799– –2809 (2001).

[47] M. Elstnera, P. Hobza, J. Heyrovsky, T. Frauenheim, S. Suhai, and E. Kaxiras, J. Chem. Phys. **114**(12), 5149– –5155 (2001).

[48] S. Grimme, J. Antony, S. Ehrlich, and H. Krieg, J. Chem. Phys. **132**(15), 154104 (2010).

[49] R. Yoshimoto, K. Hara, K. Okumura, N. Katada, and M. Niwa, J. Phys. Chem., C **111**(3), 1474–1479 (2007).

[50] M. Fischer, Microporous Mesoporous Mater. **219**, 249–257 (2016).

[51] H. Jabraoui, E. Hessou, S. Chibani, L. Cantrel, S. Lebégue, and M. Badawi, Applied Surface Science **485**, 56 – 63 (2019).

Graphical Table of Contents

GTOC image:

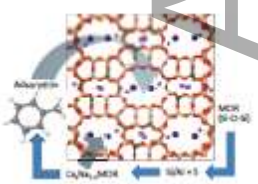

A theoretical and experimental investigation of the adsorption of toluene in doped sodium and cesium mordenite are performed. A sequential incorporation of alcaline extraframework from

pure Na up to pure Cs was done. We found that the incorporation of Cs enhances the adsorption ability of the zeolite. Mostly of the adsorption situations occurs when the electrons of the aromatic ring can interact with the counterions inside the main channel.

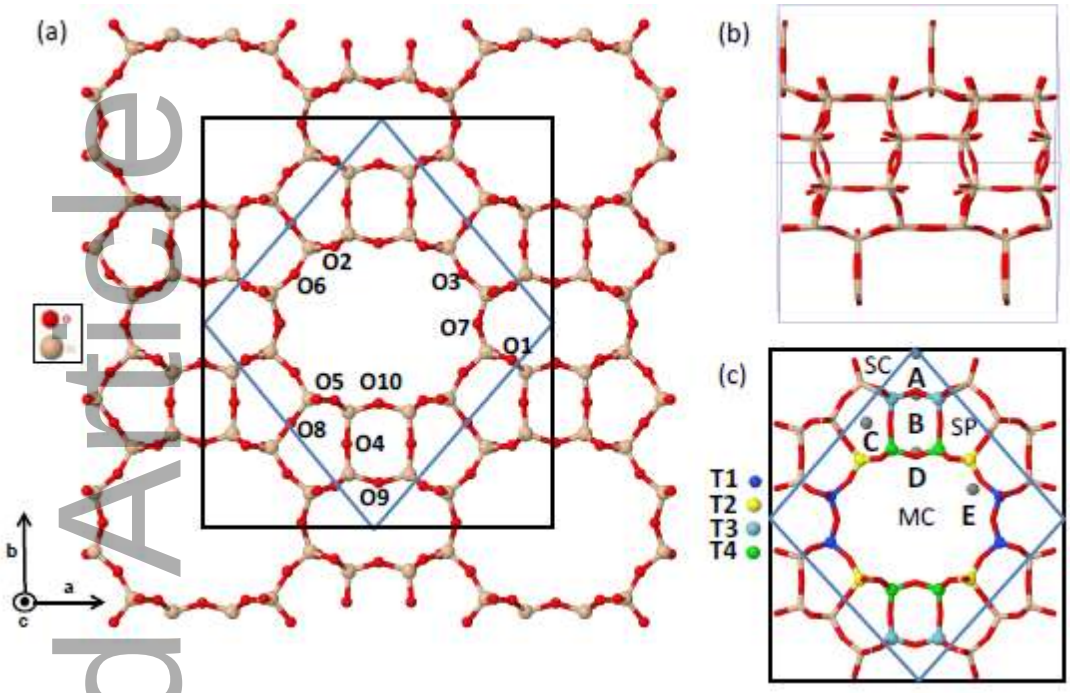

Figure 1 Crystalline structure of the mordenite. (a) Main and secondary channels. Rectangular box indicates the unit cell. Rhomboidal box represents the primitive cell. (b) Lateral view of the primitive cell used, twice the minimal cell by duplicating it along c^- axis. (c) Front view of the primitive cell. With different colors are identified the nonequivalent tetrahedra in the structure. A-E (or equivalently MC, SC, and SP) are the possible locations for the cations.

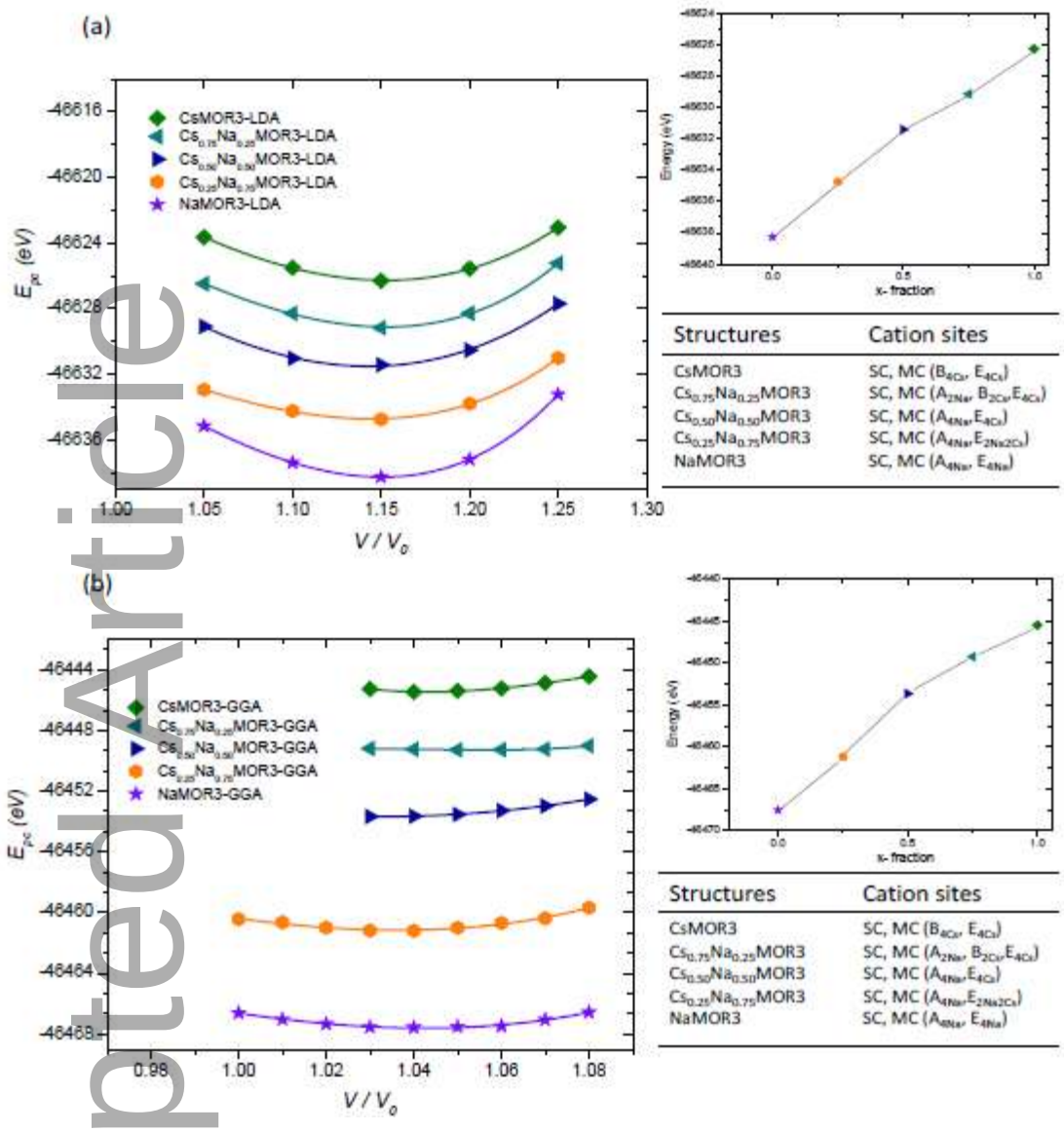

Figure 2 Total energy per primitive cell of Cs_xNA_{1-x}MOR. V_0 is the volume from IZA database distances [37]. a) LDA aproximation . b) GGA aproximation. Right panel shows the energy for optimal cell volume for each structure in function of x-fraction. The tables indicate the final position of the counterions after the dynamical simulation. In all the cases the counterions are placed in MC and SC sites. The solid lines are the fitting curves with the Birch–Murnaghan equation of state [44, 45].

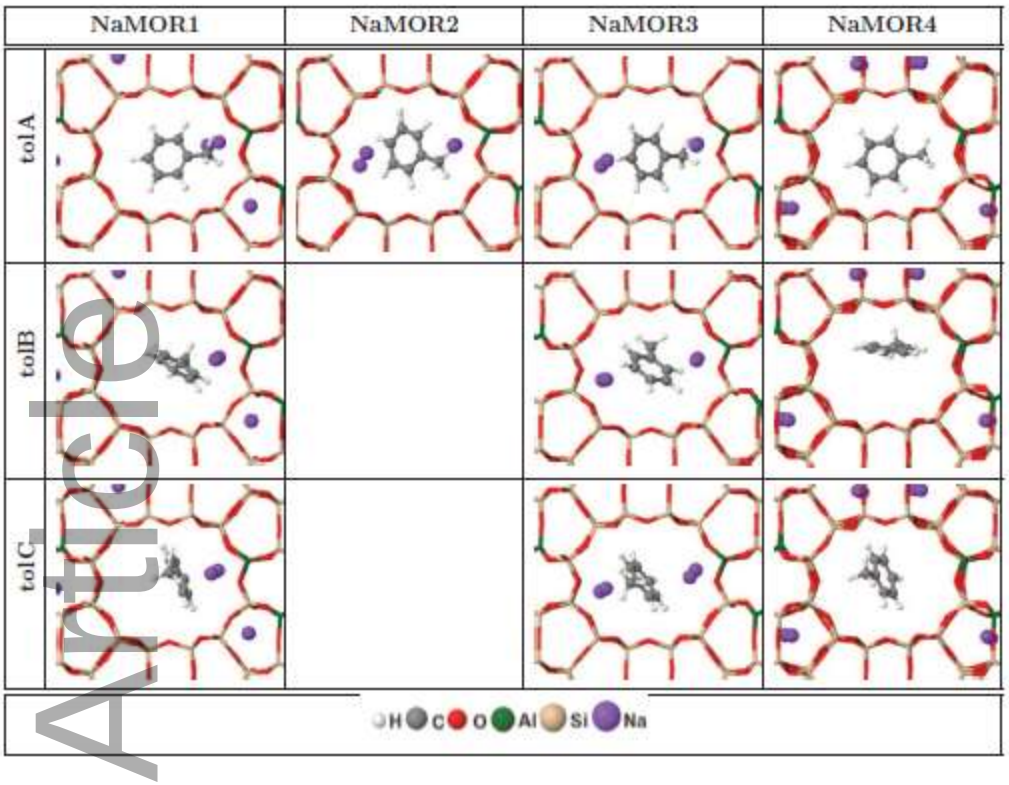

Figure 3 Final geometries for the adsorption of toluene in four different NaMOR models in the tolA, tolB and tolC position, respectively. The closest distance between sodium atoms inside the MC for the four structures is 7.52 Å

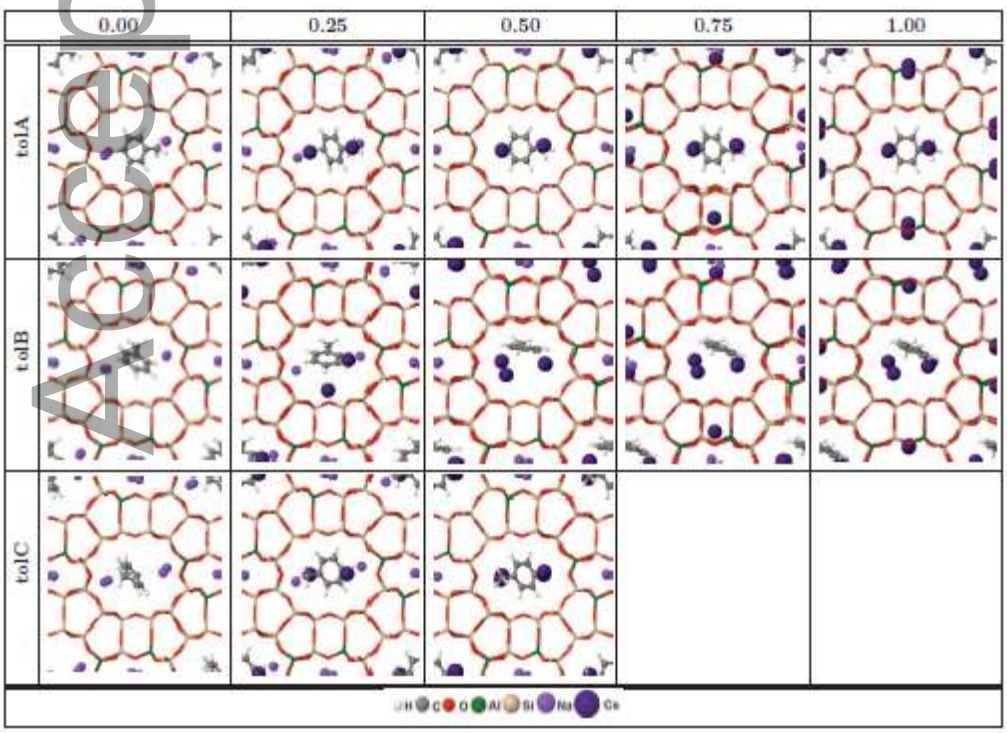

Figure 4 Final geometries for the adsorption of toluene in different concentrations of Na- and CsMOR in the tolA, tolB and tolC positions, respectively. The closest distance between counterions inside the MC for the all the structures is 4.26 Å

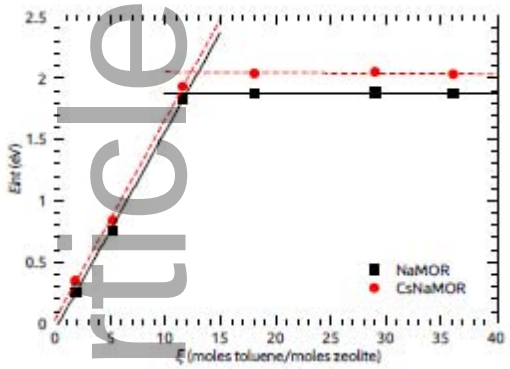

Figure 5 Interaction or desorption energy as a function of the amount of toluene.

Table 1: Interatomic distances (in Å) and relative angles for the principal tetrahedra in a fully siliceous mordenite structure.

	fireb.	fireb.	PW	PW	Cluster
	LDA	GGA	LDA	GGA	VNW
			[20]	[20]	[21]
Distances					
T1-O1	1.69	1.62	1.61	1.63	1.64
T1-O3	1.69	1.61	1.60	1.62	1.63
T1-O6	1.70	1.62	1.61	1.62	1.64
T1-O7	1.70	1.62	1.61	1.63	1.63
Average	1.69	1.62	1.61	1.63	1.64
T3-O1	1.69	1.62	1.61	1.63	1.64
T3-O4	1.70	1.62	1.61	1.62	1.63

T3-O9	1.67	1.62	1.61	1.62	1.64
Average	1.69	1.62	1.61	1.62	1.64
Angles					
O1-T1-O3	111.6	112.4	110.9	110.9	
O1-T1-O6	107.1	107.3	108.8	108.9	
O1-T1-O7	110.4	108.0	109.3	109.3	
O3-T1-O6	110.1	107.8	109.4	109.7	
O3-T1-O7	107.8	107.8	108.0	107.7	
O6-T1-O7	109.8	113.3	110.4	110.2	
Average	109.5	109.4	109.5	109.4	
Angles					
O1-T3-O1	112.3	111.4	110.8	111.3	
O1-T3-O4	106.7	108.5	108.4	108.3	
O1-T3-O9	110.1	107.8	109.3	109.0	
O4-T3-O9	110.4	108.7	110.6	110.9	
Average	109.9	109.1	109.5	109.5	

Table 2: Relative stabilization energy $\Delta E_{rel} = E_x - E_{II}$ (x : I-VI) for different combinations of tetrahedra and Si/Al = 5 ratio. The values are in eV.

Structure	Tetrahedral	ΔE_{rel}	ΔE_{rel}
		LDA	GGA
I	T1, T2	61	59
II	T1, T3	0	0
III	T1, T4	35	14

IV	T2, T3	57	18
V	T2, T4	34	28
VI	T3, T4	37	11

Table 3: Counterions sites and relative energy $\Delta E_{rel} = E_x - E_3$ (x : 1-4) per cell (in eV) in NaMOR.

	Sites	Sites	ΔE_{rel}	ΔE_{rel}
	LDA	GGA	LDA	GGA
NaMOR1	SC, SP,MC	SC,SP,MC	4.02	0.61
	(A_4, C_2, E_2)	(A_4, C_2, E_2)		
NaMOR2	SC,MC	SC, MC	0.61	0.29
	(A_4, E_4^*)	(A_4, E_4)		
NaMOR3	SC, MC	SC, MC	0.00	0.00
	(A_4, E_4)	(A_4, E_4)		
NaMOR4	SC, SP	SC, SP	2.45	1.00
	(A_4, C_4)	(A_4, C_4)		

Table 4: Equilibrium interatomic distances (in Å) for the principal tetrahedra in different models of sodium exchanged mordenites. The first and second column corresponds to averaged values among the four models studied, NaMOR1, NaMOR2, NaMOR3 and NaMOR4, respectively.

	Average	Average	Plane	Plane	Cluster	Nat.	Synt.

	LDA	GGA	waves	waves			
	this work	this work	LDA [20]	GGA [20]	VNW [21]	MOR [42]	MOR [43]
T1-O1	1.835	1.738	1.623	1.639	1.639	1.616	1.623
T1-O3	1.778	1.765	1.589	1.601	1.629	1.605	1.609
T1-O6	1.813	1.795	1.616	1.633	1.641	1.616	1.620
T1-O7	1.805	1.731	1.617	1.632	1.634	1.628	1.629
Average	1.808	1.758	1.611	1.626	1.636	1.616	1.620
T3-O1	1.808	1.774	1.747	1.767	1.649	1.644	1.634
T3-O4	1.853	1.727	1.723	1.731	1.625	1.622	1.612
T3-O1*	1.818	1.725	1.747	1.767	1.649	1.644	1.634
T3-O9	1.778	1.754	1.763	1.786	1.646	1.644	1.632
Average	1.814	1.745	1.745	1.763	1.642	1.639	1.628

Table 5: Adsorption energies of toluene for the three adsorption geometries on four different mordenite models.

		LDA		GGA	
		E_{ads}	E_{ads}^{corr}	E_{ads}	E_{ads}^{corr}
		(eV)	(eV)	(eV)	(eV)
NaMOR 1	tolA	-0.96	-1.74	-0.82	-1.75
	tolB	-0.47	-1.12	-2.83	-3.68
	tolC	-0.62	-1.19	-3.18	-3.98
NaMOR 2	tolA	-1.16	-1.95	-2.49	-3.41
	tolB	-	-	-3.82	-4.71
	tolC	-	-	-3.81	-4.69
NaMOR 3	tolA	-0.73	-1.54	-2.96	-3.92
	tolB	-0.44	-1.14	-2.72	-3.66
	tolC	-0.54	-1.20	-2.96	-3.57
NaMOR 4	tolA	-0.33	-1.08	-0.70	-1.55
	tolB	-0.14	-0.81	0.06	-0.50
	tolC	-0.03	-0.61	-0.14	-0.71
Overall average		-0.54	-1.25	-2.20	-3.01

Table 6: Adsorption energies of the toluene on Cs_xNA_{1-x} MOR3 $(x = 0.25, 0.50, 0.75, 1)$.

		LDA		GGA	
		E_{ads}	E_{ads}^{corr}	E_{ads}	E_{ads}^{corr}
		(eV)	(eV)	(eV)	(eV)
$x = 0.25$	tolA	-1.73	-2.59	-3.16	-4.09
	tolB	-1.04	-1.74	-2.78	-3.78
	tolC	-1.60	-2.36	-3.12	-3.91
Average		-1.46	-2.23	-3.02	-3.93
$x = 0.50$	tolA	-1.75	-2.59	-3.35	-4.30
	tolB	-0.28	-1.03	-2.63	-3.38
	tolC	-0.95	-1.69	-3.33	-4.12
Average		-1.00	-1.77	-3.10	-3.93
$x = 0.75$	tolA	-1.22	-2.00	-3.20	-4.14
	tolB	0.25	-0.40	-2.54	-3.28
	tolC	-	-	-3.22	-3.99
Average		-0.48	-1.20	-2.98	-3.80
$x = 1$	tolA	-1.30	-2.23	-3.64	-4.59
	tolB	-0.07	-0.82	-2.85	-3.60
	tolC	-	-	-3.57	-4.34
Average		-0.68	-1.52	-3.36	-4.18